

Quantum oscillations and Berry's phase in topological insulator surface states with broken particle-hole symmetry

Anthony R. Wright* and Ross H. McKenzie

School of Mathematics and Physics, University of Queensland, Brisbane, 4072 Queensland, Australia

(Dated: October 17, 2018)

Quantum oscillations can be used to determine properties of the Fermi surface of metals by varying the magnitude and orientation of an external magnetic field. Topological insulator surface states are an unusual mix of normal and Dirac fermions. Unlike in graphene and simple metals, Berry's geometric phase in topological insulator surface states is not necessarily quantized. We show that reliably extracting this geometric phase from the phase offset associated with the quantum oscillations is subtle. This is especially so in the presence of a Dirac gap such as that associated with the Zeeman splitting or interlayer tunneling. We develop a semi-classical theory for general mixed normal-Dirac systems in the presence of a gap, and in doing so clarify the role of topology and broken particle-hole symmetry. We propose a systematic procedure of fitting Landau level index plots at large filling factors to reliably extract the phase offset associated with Berry's phase.

PACS numbers: 73.25.+i, 72.20.Fr, 73.43.Qt

I. INTRODUCTION

Topological insulators are bulk insulators with metallic surface states that are topologically protected¹⁻³. The quantized Hall resistance in two-dimensional topological insulators was measured several years ago^{4,5}. Recently measurements have been made of properties of the surface states of three-dimensional topological insulators. Angle Resolved PhotoEmission Spectroscopy (ARPES) studies provide direct imaging of near-surface bands^{6,7} showing dispersions of an odd number of Dirac cones, as expected for a topological insulator. Furthermore, these band structures are consistent with the presence of a non-trivial Berry's phase of π .⁸ However, these surface band structures also exhibit significant band-bending, and particle-hole symmetry with respect to the Dirac point is broken.

A complementary method to ARPES to determine the Fermi surface properties of a metal is to measure quantum oscillations such as associated with the Shubnikov de Haas or de Haas van Alphen effects.⁹ Such experiments can distinguish between bulk and surface states, even if both are gapless (or near-gapless), by tilting the magnetic field¹⁰. Furthermore, the phase offset (γ) of the quantum oscillations is related to the Berry's phase associated with cyclotron orbits and provides a means to experimentally access this important signature of a Dirac cone. Experiments on graphene^{11,12} found evidence of the expected non-trivial Berry's phase of π . There have now been a number of quantum oscillation experiments on 3D topological insulators.^{10,13-24} A prevalent observation in these studies is that the phase offset is not equal to the zero value associated with a Berry's phase of π . In Table I we have listed the different phase offsets obtained by various groups and materials. The deviation of the observed γ from zero has been variously attributed to the Zeeman effect^{14,25}, and the non-ideal Dirac (i.e. nonlinear) nature of the surface states.²⁶ In the present work, we reformulate both of these proposals in a precise

and concrete manner.

Material	$B_0(T)$	γ	Ref.
Bi _{0.91} Sb _{0.01}	0.65	0.25	13
Bi ₂ Se ₃ (S2)	32	-0.5	14
Bi ₂ Se ₃ (S3)	100	-0.7	14
Bi ₂ Te ₂ Se	64	0.22 ± 0.12	15
Bi ₂ Te ₃	50	-0.05 ± 0.05	18
Bi ₂ Se ₃	16	-0.15 ± 0.08	19
Bi ₂ Te ₂ Se (S1)	60	0.05 ± 0.02	20
Bi ₂ Te ₂ Se (S4)	47	0.32	20
Bi ₂ Te ₂ Se	73	-0.05	21
Bi ₂ Se ₃	many	-0.1 ± 0.1	22
Bi _{1.996} Sn _{0.004} Te ₂ Se	116	-0.1 ± 0.1	24
graphene	44	0	11

TABLE I: The different phase offsets (γ) measured for various materials and at various chemical potentials (quantified by the frequency of the quantum oscillations (B_0), the surface area of the cyclotron orbit in teslas). The second last entry was performed at more than 20 different chemical potentials. S# denotes the sample number in the experiment.

The aim of this Article is to provide a quantitative framework for using quantum oscillation experiments to characterise topological insulator surface states. In particular, we focus on extracting the phase offset and the cyclotron effective mass from experiments. For mixed normal-Dirac systems (i.e. Dirac cones with a particle-hole symmetry breaking quadratic term), we find that there is a key energy scale relevant to quantum oscillation experiments: the normal fermion mass multiplied by the Dirac Fermi velocity squared, mv_F^2 . The interplay of this energy scale with the Zeeman or intrinsic Dirac-gap (Δ) introduces subtleties to quantum oscillations that both complicate and enrich the observed phenomena. In particular, we find that the phase offset is only quantized if the system is either gapless or particle-hole symmetric.

In a topological insulator surface state under an applied magnetic field, the phase offset is *never* independent of magnetic field because of the Dirac mass gap associated with the Zeeman splitting, together with the ubiquitous particle-hole symmetry breaking. We outline how one can circumvent this difficulty: by fitting the experimental data at large filling factors to a simple function (Eq. (36)), one can obtain a linearized form which is asymptotically exact in zero field. The intercept of such a linear plot as $1/B \rightarrow 0$ yields the topologically relevant phase offset at zero field. We hope that this analysis will be valuable to future experimental studies, and will stimulate further studies utilising quantum oscillation experiments to investigate other topological insulator regimes, such as associated with thin films.^{27,28}

The structure of the article is as follows. In Sec. II, we develop the semiclassical theory of quantum oscillations when particle-hole symmetry is broken. In Sec III, we introduce a specific model Hamiltonian. In Sec. IV, we analyse the quantum oscillations in the model system, and focus on the non-universal phase offsets and the subtleties of cyclotron effective mass measurements. This section ends with an analysis of expected Landau level index plots in these experiments. In Sec. V, we propose a robust procedure to extract the phase offset from experiment, overcoming the difficulties which led to the wide range of values in Table I. In Sec. VI we compare our results with existing experiments and show that the procedure outlined in the preceding section can substantially improve phase offset measurements. In Sec. VII, we comment briefly on the relevance of our results to spintronic systems.

II. SEMICLASSICAL THEORY OF QUANTUM OSCILLATIONS

By measuring the longitudinal resistivity of a metal sample as a function of external field strength B , one observes that it oscillates according to⁹

$$\Delta\rho_{xx} \propto \cos\left[2\pi\left(\frac{B_0}{B} - \gamma\right)\right], \quad (1)$$

where the oscillation frequency, B_0 , is related to the area of the Fermi surface enclosed by the cyclotron orbit, and γ is a phase offset. This is the Shubnikov–de-Haas effect. The de-Haas–van-Alphen effect, which is the oscillation of the magnetisation of a sample as a function of B takes a similar form, and in two dimensions is given by Eq. (14). The phase offset, γ is related to the Berry’s phase of the cyclotron orbit.²⁹ A key issue we clarify in the present work is the role of the Berry’s phase in the phase offset γ .

A. The phase offset in quantum oscillations

Under a weak external magnetic field, electrons follow equi-energy contours about the electronic dispersion. In order to construct a semi-classical theory of this situation, one usually begins with Onsager’s semi-classical quantisation condition due to the single-valuedness of Bloch wavefunctions³⁰. The k -space area $S(C)$ of a closed electronic orbit C is quantized according to

$$S(C)l_B^2 = 2\pi(n + \gamma(C)) \quad (2)$$

where l_B is the magnetic length, defined by $l_B = \sqrt{\hbar/eB}$, and n is an integer. The phase offset $\gamma(C) = 1/2 - \Gamma(C)/2\pi$, with $\Gamma(C)$ the Berry’s phase of the orbit C ^{31,32}, given by

$$\Gamma_\alpha(C) = i \oint_C d\mathbf{k} \cdot \langle u_{\mathbf{k},\alpha} | \nabla_{\mathbf{k}} u_{\mathbf{k},\alpha} \rangle. \quad (3)$$

in the band α . This is expressed in terms of the eigenvectors $|u_{\mathbf{k},\alpha}\rangle$ of the k -dependent Hamiltonian

$$H(\mathbf{k}) = \exp(-i\mathbf{k} \cdot \mathbf{r})H \exp(i\mathbf{k} \cdot \mathbf{r}), \quad (4)$$

where H is, say, a tight-binding Hamiltonian. For normal fermions with a quadratic dispersion, or in fact any isolated band, $\Gamma(C) = 0$ for any contour C . For massless Dirac fermions, the Berry’s phase is again path independent, giving $\Gamma(C) = \pi$. Accounting only for the bare dispersion contribution to the cyclotron orbit, it is tempting to take C to be the equi-energy closed path of the zero-field dispersion. Thus $\gamma(C)$ for a contour which includes only the bare dispersion contribution to the energy gives a constant $\gamma = 1/2$ for normal fermions, and $\gamma = 0$ for massless Dirac fermions³³. However, for massive Dirac fermions the dispersion is no longer linear at low energies, and the Berry’s phase is no longer path independent, (i.e. $\Gamma = \Gamma(C)$), and so $\gamma(C)$ is not, in general, quantized.²⁹

In a clear and insightful recent article, Fuchs *et al.*²⁹ pointed out that for a massive Dirac cone in a magnetic field, there is a pseudo-spin orbital magnetic moment contribution to the energy that must be taken into account for cyclotron orbits (*i.e.* equi-energy contours). The Onsager condition for cyclotron orbits is generalised in this case to

$$S(\epsilon)l_B^2 = 2\pi(n + \gamma_\alpha(\epsilon)). \quad (5)$$

The quantity $\gamma_\alpha(\epsilon)$ is not, in general, equal to $\gamma(C)$, since it also includes the pseudo-spin magnetisation component. It is $\gamma_\alpha(\epsilon)$ that gives the relevant phase offset, and not $\gamma(C)$ in Eq. (5).

Somewhat surprisingly, for the particle-hole symmetric massive Dirac cone, this extra contribution to the phase offset due to the pseudo-spin orbital magnetic moment exactly cancels the energy-dependent part of the Berry’s

phase, such that $\gamma_\alpha(\epsilon) = 0$ after all.²⁹ By inverting Eq. (5), it can be shown that the semi-classical Landau levels exactly reproduce the fully quantum mechanical ones in the specific case of a massive Dirac cone. For this reason, Fuchs *et al.* label $\gamma_\alpha(\epsilon)$ (γ_L in their nomenclature) the ‘Landau index shift’, and they associate it with a winding number of the orbit – a topological quantity. Therefore, the phase offset is strictly $\gamma = 1/2$ for normal fermions, and $\gamma = 0$ for particle-hole symmetric Dirac fermions.

B. A general expression for the phase offset in quantum oscillations: broken particle-hole symmetry

A further goal of this work is to generalise the contribution of Fuchs *et al.* to systems with broken particle-hole symmetry. This extension applies to many systems, most notably at present, topological insulator surface states^{34,35}. We find that in the case of broken particle-hole symmetry, the winding number can no longer be associated with the magnetic moment-adjusted Berry’s phase, and so the strict quantisation of $\gamma_\alpha(\epsilon)$ is removed.

Consider a general two band system. Following Fuchs *et al.*,²⁹ the energy of an electron in band α is

$$\epsilon_\alpha(\mathbf{k}) = \epsilon_{0,\alpha}(\mathbf{k}) - \mathcal{M}_\alpha(\mathbf{k}) \cdot \mathcal{B}, \quad (6)$$

where $\epsilon_{0,\alpha}(\mathbf{k})$ is the bare dispersion energy in zero field, \mathcal{B} is the external magnetic field, and the pseudo-spin orbital magnetic moment^{29,32}

$$\begin{aligned} \mathcal{M}_\alpha(\mathbf{k}) &= \frac{e}{2} \langle (\hat{\mathbf{r}} - \mathbf{r}_c) \times \hat{\mathbf{j}} \rangle \\ &= \frac{e}{2\hbar} (\epsilon_{0,\alpha}(\mathbf{k}) - \epsilon_{0,\bar{\alpha}}(\mathbf{k})) \Omega_\alpha(\mathbf{k}), \end{aligned} \quad (7)$$

where \mathbf{r}_c is the centre of mass position of the wavepacket, $\hat{\mathbf{j}}$ is the current operator, and $\bar{\alpha}$ denotes the band which is not α . We emphasise that Eq. (7) is a property of Bloch electrons in a magnetic field, and has nothing to do with spin. $\Omega_\alpha(\mathbf{k})$ is the Berry curvature which is the local quantity given by

$$\Omega_\alpha(\mathbf{k}) = \nabla_{\mathbf{k}} \times i \langle u_{\mathbf{k},\alpha} | \nabla_{\mathbf{k}} u_{\mathbf{k},\alpha} \rangle \quad (8)$$

and is related to the Berry’s phase by Stokes’ theorem such that

$$\Gamma_\alpha(C) = \int_S \Omega_\alpha(\mathbf{k}) d\mathbf{k}, \quad (9)$$

where S is the area enclosed by C . Eq. (7) generalizes Appendix C in Ref.(29) to the case of broken particle-hole symmetry. Including the magnetic moment in Eq. (5), we can obtain the full quantisation condition for a generic two-band model, by finding

$$\begin{aligned} S(\epsilon_{0,\alpha}(\mathbf{k})) l_B^2 &= S(\epsilon_\alpha(\mathbf{k}) + \mathcal{M}_\alpha(\mathbf{k}) \cdot \mathcal{B}) l_B^2 \\ &\approx S(\epsilon_\alpha(\mathbf{k})) l_B^2 + \frac{1}{2} (\epsilon_\alpha(\mathbf{k}) - \epsilon_{\bar{\alpha}}(\mathbf{k})) \frac{d\Gamma_\alpha(\epsilon)}{d\epsilon_\alpha(\mathbf{k})}. \end{aligned} \quad (10)$$

In the last equality we made use of Eq. (7) and Eq. (9). Rearranging the above expression to obtain $S(\epsilon_\alpha(\mathbf{k}))$, and recognising that we already know $S(\epsilon_{0,\alpha}(\mathbf{k}))$ from Onsager’s condition, Eq. (5) we obtain

$$\gamma_\alpha(\epsilon) = \frac{1}{2} - \frac{1}{2\pi} \left[\Gamma_\alpha(\epsilon) + \frac{1}{2} (\epsilon_{0,\alpha} - \epsilon_{0,\bar{\alpha}}) \frac{d\Gamma_\alpha(\epsilon)}{d\epsilon_{0,\alpha}} \right]. \quad (11)$$

This result for the phase offset in particle hole symmetry broken mixed Dirac-normal fermion systems directly leads to Eq. (26), the central result of this paper. Two limiting cases are worth mentioning. Firstly, for particle-hole symmetric Hamiltonians, $\epsilon_{0,\bar{\alpha}} = -\epsilon_{0,\alpha}$, and the second and third terms on the right together reduce to a multiple of the winding number already obtained by Fuchs *et al.*, which is simply 1/2, giving $\gamma_\alpha(\epsilon) = 0$. Secondly, for a degenerate two band system, $\epsilon_{0,\bar{\alpha}} = \epsilon_{0,\alpha}$, and $\Gamma = 0$, trivially giving $\gamma_\alpha(\epsilon) = 1/2$. In general, however, no such simplification is possible.

C. Semi-classical theory of the de-Haas–van-Alphen effect

The Lifshitz-Kosevich theory of the de-Haas van-Alphen effect for a single species of free electrons has been obtained by Champel and Mineev⁹. Starting from an expression for the Green’s function of an electron in a magnetic field, they obtain the density of states, and then the thermodynamic potential. From here one can directly obtain the magnetization, and see that it oscillates as a function of magnetic field. In particular, this demonstrates the direct relation between oscillations in density of states as a function of field strength, and how they directly lead to oscillations in magnetization.

By inverting Onsager’s condition, Eq. (5), in terms of energy levels, and thus replacing the energy levels in a magnetic field with an expression for the quantized orbits $S(\epsilon)$ and the phase offset γ , Luk’yanchuk and Kopelevich³⁶ generalised the treatment of the de-Haas–van-Alphen (dHvA) semiclassically, for arbitrary systems.

In a magnetic field, the electrons in band α undergo cyclotron orbits with frequency

$$\omega_c(\epsilon_\alpha) = \frac{eB}{m_\alpha^*(\epsilon)}, \quad (12)$$

where the cyclotron effective mass is

$$m_\alpha^*(\epsilon) = \frac{1}{2\pi} \frac{dS_\alpha(\epsilon)}{d\epsilon_\alpha}. \quad (13)$$

The 2D result obtained by Luk'yanchuk and Kopelevich³⁶ of which we are interested here, is given by

$$M_{osc} = \sum_{\alpha} \frac{-e}{\pi^2 \hbar^2} \frac{S_{\alpha}(\epsilon)}{dS_{\alpha}(\epsilon)/d\epsilon} \sum_{l=1}^{\infty} \frac{\lambda}{\sinh(\lambda l)} e^{-\frac{2\pi l}{\omega_c \tau}} \times \sin\left(2\pi l \left[\frac{S_{\alpha}(\epsilon)}{2\pi \hbar e B} - \gamma_{\alpha}(\epsilon) \right]\right) \cos\left(2\pi l \frac{g_s \mu_B B}{\hbar \omega_c}\right) \quad (14)$$

where

$$\lambda = \frac{2\pi^2 k_B T}{\hbar \omega_c} \frac{dS(\epsilon)}{d\epsilon} \quad (15)$$

and \hbar/τ is the Landau level broadening.

Quantum oscillations provide an experimental method to determine $\gamma_{\alpha}(\epsilon)$. By assigning integers (n) to the oscillation maxima/minima in the magnetisation or resistance as a function of inverse field, one can extrapolate these to $1/B \rightarrow 0$ to obtain $\gamma_{\alpha}(\epsilon)$ which is the n -intercept, Modulo 1.

III. TOPOLOGICAL INSULATOR SURFACE STATES

A. Model Hamiltonian

Consider a two-band Hamiltonian, where the basis is not necessarily spin, but can be thought of as a pseudo-spin, and may be spin, sub-lattice, on-site orbitals, etc, and which contains both normal fermions, and massive Dirac fermions, given by^{25,34,35,37}

$$H = \left(\frac{\hbar^2 k^2}{2m} - \mu \right) \mathbf{I}_2 + \begin{pmatrix} \Delta & \hbar v_F (k_y + i k_x) \\ \hbar v_F (k_y - i k_x) & -\Delta \end{pmatrix} \quad (16)$$

where there are four free parameters, m , μ , v_F , and Δ . m is the mass associated with the normal part of the spectrum, μ is the chemical potential, v_F is the velocity of the Dirac part of the spectrum, and Δ is the Dirac gap.

This Hamiltonian, at $\Delta = 0$, is the low energy surface theory of a time reversal invariant topological insulator. Following the classification scheme outlined by Schnyder *et al.*³⁸, we see that the quadratic term breaks particle-hole and chiral, or sub-lattice symmetries. Since we are concerned with electrons then, time reversal is antilinear, and the subclass of the topological insulator is AII, and the topological number is a \mathcal{Z}_2 invariant. Generically, finite Δ gives a Dirac mass gap, and so the three dimensional system is no longer a topological insulator.

In the absence of an orbital magnetic field there are two bands, with dispersion

$$\epsilon_{\alpha}(\mathbf{k}) = \frac{\hbar^2 k^2}{2m} + \alpha \sqrt{\Delta^2 + \hbar^2 v_F^2 k^2}, \quad (17)$$

where $\alpha = \pm$.

The Landau level spectrum can be calculated exactly, giving³⁹

$$\epsilon_n^{\alpha} = \hbar \omega_0 n \pm \sqrt{2\hbar v_F^2 e B n + \left(\frac{\hbar \omega_0}{2} - \frac{g_s \mu_B B}{2} \right)^2}, \quad (18)$$

where $\omega_0 = eB/m$. In the limit $v_F \rightarrow 0$, we obtain the usual normal fermion Landau level spectrum, and in the limit $m \rightarrow \infty$, we obtain the Dirac fermion spectrum:

$$\epsilon_n = \begin{cases} \hbar \omega_0 (n + \frac{1}{2}) & \text{(Normal fermion)} \\ \sqrt{2\hbar v_F^2 e B n} & \text{(Dirac fermion)} \end{cases} \quad (19)$$

which are quoted at $\Delta = 0$. Respectively, the phase offset for quantum oscillations can be ‘read off’, as $\gamma = 1/2$ for normal fermions, and $\gamma = 0$ for Dirac fermions. In the mixed case of Eq. (18), however, there is no constant which can be so readily extracted from the Landau level expression.

We can define a useful ‘interpolation parameter’, given by

$$\eta \equiv \frac{m v_F^2}{m v_F^2 + \mu}, \quad (20)$$

which for $\mu, m > 0$ gives $0 \leq \eta \leq 1$. The interpolating parameter gives as two limiting cases at finite μ :

$$\eta = \begin{cases} 0, & v_F \rightarrow 0 \text{ (Normal fermion)} \\ 1, & m \rightarrow \infty \text{ (Dirac fermion)}. \end{cases} \quad (21)$$

Generally, η small gives a Rashba spin orbit coupled 2DEG,³⁷ where v_F is the Rashba spin splitting, and $\Delta = g_s \mu_B B$ is the Zeeman splitting; $\eta \approx 1$ gives, for example, graphene at $\Delta = 0$, and boron nitride at $\Delta \neq 0$,^{11,40} and $0 < \eta < 1$ gives the surface states of topological insulators^{34,35}, where Δ can be the Zeeman splitting or a tunnel splitting for thin films⁴¹. Although we are most interested in the latter regime, our results are generally valid for all values of η and Δ .

B. Broken particle-hole symmetry

In real materials topological insulator (TI) surface states are not simply described by massless Dirac cones. ARPES experiments show surface states with significant band-bending and broken particle-hole symmetry with respect to the band crossing point^{15,42,43}. For this reason, Hamiltonian Eq. (16) is the relevant low energy Hamiltonian to describe topological insulator surface states. This has been confirmed by symmetry arguments^{34,35}. In Table II, we show some of the values for the mass m , and the Fermi velocity v_F characterising the Hamiltonian Eq.

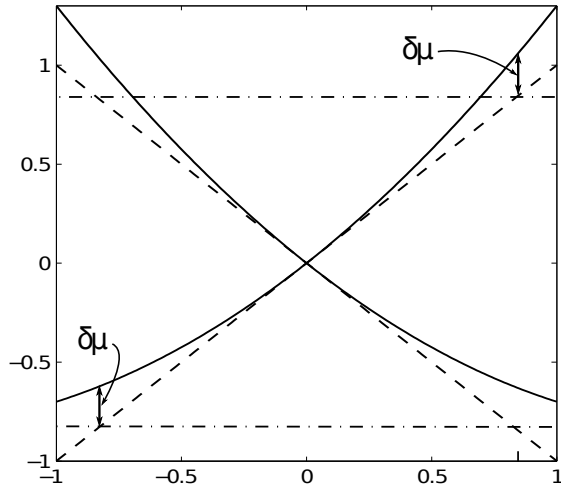


FIG. 1: Model band structure with particle-hole asymmetry, highlighting the effect of the $p^2/2m$ term relative to the chemical potential. In a particle-hole symmetric system, $\epsilon_+(k) = -\epsilon_-(k)$. At finite m , away from $k = 0$, the chemical potential is shifted up for either band with respect to the symmetric case, by an amount $\delta\mu/\mu \approx \mu/(2mv_F^2) = (1/\eta - 1)/2$. In the limit $\mu \rightarrow 0$ or $m \rightarrow \infty$, the shift $\delta\mu/\mu \rightarrow 0$, restoring particle-hole symmetry.

(16) measured by ARPES. It is clear from this data that for typical doping levels, the topological insulator surface states are truly mixed normal-Dirac systems, and cannot be considered to be approximating either regime.

Material	m/m_e	v_F (ms ⁻¹)	μ (meV)	η	Ref.
Bi ₂ Se ₃	0.25	5.0×10^5	300	0.54	42
Bi ₂ Te ₂ Se	0.13	3.4×10^5	130	0.39	15
Bi ₂ Te ₃	3.8	3.9×10^5	250	0.93	43
Bi _{1.5} Sb _{0.5} Te _{1.7} Se _{1.3}	0.32	4.6×10^5	140	0.73	16

TABLE II: Estimates of model Hamiltonian parameters for several 3D topological insulator materials. Normal fermion mass m and Dirac fermion Fermi velocities v_F are estimated from ARPES. At the values of the chemical potential μ quoted in these works, we have also calculated the parameter η , defined in equation Eq. (20).

The effect of broken particle hole symmetry on the transport properties of topological insulators has been investigated theoretically,⁴⁴ and experimentally.⁴⁵

We can think of the two limiting cases of Eq. (21) in terms of particle-hole symmetry. In particular, pure Dirac fermions have particle-hole symmetry for all μ , whereas pure normal fermions have two degenerate bands and so have broken particle-hole symmetry for all μ . For

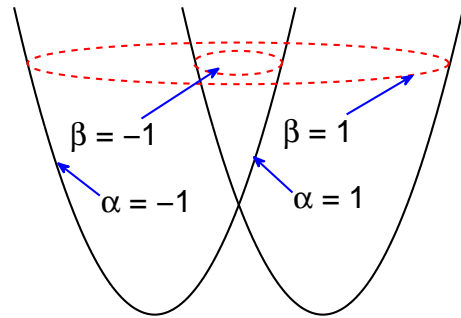


FIG. 2: For all energies, there are two distinct cyclotron orbits (Fermi surfaces). However, for real materials the Hamiltonian Eq. (16) is an effective one for low energies, and the outer orbit may not actually exist. Nevertheless, for systems with small η , such as Rashba systems,³⁷ there are two possible orbits, indexed by $\beta = \pm 1$ for outer and inner orbits. In the figure, $\mu > 0$, so the inner orbit ($\beta = -1$) circulates around the $\alpha = 1$ band, and the outer ($\beta = 1$) orbit circulates around the $\alpha = -1$ band. For $\mu < 0$, both orbits circulate around the $\alpha = -1$ band.

$0 < \eta < 1$, the system is neither purely Dirac nor purely normal, but is a mixture of the two. In particular, near $k = 0$, for any finite η , the electrons are Dirac fermion-like, and far away from $k = 0$, they become normal fermion-like. We can rearrange Eq. (21) to quantify this statement in terms of μ

$$\frac{\mu}{mv_F^2} = \frac{1}{\eta} - 1. \quad (22)$$

We can say that η provides a measure of broken particle-hole symmetry with respect to $k = 0$. The effect of broken particle-hole symmetry on the band-structures is elucidated in Fig. 1.

C. Gap opening: Zeeman and tunnel splitting, and beyond

Mikitik and Sharlai have argued that, in general, for Bismuth-based 3D topological insulators, $\gamma = 0$ in the weak field limit.⁴⁶ It has been shown that the symmetries of the Bismuth based TIs don't allow for a non-zero gap Δ in Eq. (16)^{34,35}, and so apart from the Zeeman splitting, and as we shall show, γ is strictly zero.

However, it is clear from Table I that γ is rarely observed to be zero, but in fact deviates substantially from zero. This implies that the g-factor may be $\sim 10 - 100$ in topological insulator surface states^{14,26}. This corresponds to a Zeeman gap of 6 - 60 meV in a 10T field, which, when compared to typical Fermi energies of 50 - 300 meV (Table I), is not insignificant.

In topological insulator thin films, the surface states on the two faces of the sample hybridise, and thus open a

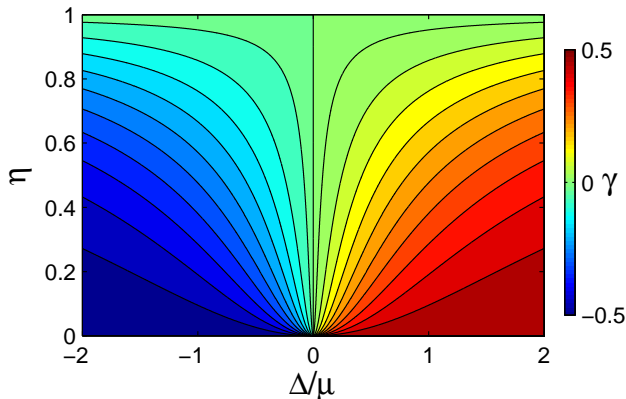


FIG. 3: (Color online) The phase offset γ_+ as a function of Δ , the gap parameter, and η , the dimensionless parameter that tunes between normal fermions ($\eta = 0$) and Dirac fermions ($\eta = 1$). It is this quantity, and not simply the Berry's phase, that determines the phase offset in quantum oscillation experiments. If *either* particle-hole symmetry is maintained ($\eta = 0, 1$), or the system is gapless, the phase offset is a constant. If neither condition applies, the phase offset is a continuous function of η and Δ . The solid lines denote constant values of γ_+ .

gap⁴¹. So even in Bismuth-based TIs, a non-zero Δ in Eq. (16) can occur. In fact, thin films below the critical thickness (6 quintuple layers⁴⁷) have already been successfully produced in the lab, and the gap observed^{16,48,49}.

There are other mechanisms for gap formation which have been suggested, and even realised, including excitonic pairing gaps^{27,28} and a possible Higgs-type mechanism near the phase transition from the topological insulating phase to the topologically trivial insulating phase.⁵⁰ The formation of a gap is also crucial to various topological effects becoming manifest, including the as-yet unverified topological magneto-electric effect⁵¹.

IV. QUANTUM OSCILLATIONS IN TOPOLOGICAL INSULATOR SURFACE STATES

A. Non-universal phase offset in quantum oscillations

The Berry's phase is given by Eq. (3), and is readily calculated for the Hamiltonian Eq. (16). In particular, noting that the Berry's phase is a function of the wavefunctions only, the k^2 term in Eq. (16) does not contribute for a path at fixed momentum space radius k , and so at all η , we have

$$\Gamma_\alpha(k) = \pi\alpha \left(1 - \frac{\Delta}{\sqrt{\Delta^2 + \hbar^2 v_F^2 k^2}}\right), \quad (23)$$

which is the same result obtained in Ref.[29] for the case $m \rightarrow \infty$. At fixed energy however, $k(\epsilon)$ is deter-

mined from the full dispersion Eq. (17), and the Berry's phase at fixed energy is implicitly dependent upon the full Hamiltonian. Moreover, the $\alpha = -1$ band has both an inner and an outer orbit, as shown in Fig. 2. In particular, solving the dispersion at fixed energy ϵ for k^2 , we obtain

$$k_\beta^2 = \frac{2m}{\hbar^2} (\epsilon + mv_F^2 + \beta \sqrt{\Delta^2 + 2\epsilon mv_F^2 + m^2 v_F^4}), \quad (24)$$

where $\beta = \pm 1$. The Berry's phase and phase offset γ will then acquire an inner/outer orbit index. For $\alpha = 1$, $\beta = -1$ always, as there is no outer orbit in this case. However for $\alpha = -1$, and $\epsilon < 0$, $\beta = [-1, 1]$ coexist, and for $\epsilon > 0$, $\beta = 1$ always. At fixed energy then,

$$\Gamma_{\alpha,\beta}(\epsilon) = \pi\alpha \left[1 - \frac{\Delta}{mv_F^2 (1 + \beta \sqrt{1 + \frac{2\epsilon}{mv_F^2} + \frac{\Delta^2}{(mv_F^2)^2}})} \right] \quad (25)$$

With the Berry's phase known, we are able to find the phase offset for quantum oscillations from Eq. (11). For the inner orbits ($\beta = -1$), the relevant case for topological insulators, we obtain

$$\gamma_{\alpha,-}(\epsilon) = \frac{\alpha\Delta}{2mv_F^2 \sqrt{1 + \frac{2\epsilon}{mv_F^2} + \frac{\Delta^2}{(mv_F^2)^2}}}. \quad (26)$$

This is the central result of this paper, which shows that the phase offset expected in quantum oscillation experiments on topological insulator surface states is non-universal, but in fact depends upon the energy scales of the gap, and a mixed normal-Dirac fermion energy scale, mv_F^2 .

For the outer orbits, only relevant for the $\alpha = -1$ band, and, for example, Rashba systems where v_F is small,³⁷

$$\gamma_{-,+}(\epsilon) = \gamma_{-,-}(\epsilon) + \frac{\Delta mv_F^2}{(x + \frac{mv_F^2}{2})^2 - \frac{m^2 v_F^4}{4}}. \quad (27)$$

Where $x = \sqrt{\Delta^2 + 2\epsilon mv_F^2 + m^2 v_F^4}$. We have included this result for completeness, but from now on will focus on the inner orbits, relevant for topological insulator surface states, and drop the β index in Eq. (26).

There are three particularly interesting limiting cases:

$$\gamma_\alpha(\epsilon) = \begin{cases} \frac{1}{2}, & v_F \rightarrow 0 \text{ (Normal fermions)} \\ 0, & m \rightarrow \infty \text{ (Dirac fermions)} \\ 0, & \Delta \rightarrow 0 \text{ (Mixed gapless)} \end{cases} \quad (28)$$

The second and third limit together are particularly interesting, as they imply that for infinitesimally small v_F , at $\Delta = 0$, $\gamma = 0$, and so γ jumps discontinuously from 0 to 1/2 at $v_F = 0$. This discontinuity is apparent in the vertical line of Fig. 3 at $\Delta = 0$ as $\eta \rightarrow 0$.

The second limit gives the same result obtained previously by Fuchs *et al.*²⁹: in the presence of particle-hole symmetry and a Dirac gap the phase offset is zero, even though the Berry's phase Γ is not equal to π and varies with the chemical potential.

Fig. 3 shows the expected phase offset for the electron band of gapped systems with both normal and Dirac components in terms of the two parameters $\tilde{\Delta} = \Delta/\mu$ and η . The phase offset Eq. (26) can be written in terms of these as follows:

$$\gamma_\alpha(\Delta/\mu, \eta) = \frac{\alpha(1-\eta)\Delta/\mu}{2\sqrt{\eta(2-\eta) + (\Delta/\mu)^2(1-\eta)^2}}. \quad (29)$$

The phase offset varies as a function of the energy scale mv_F^2 . The horizontal line $\eta = 0$ corresponds to purely normal fermions, and $\eta = 1$ to purely Dirac fermions. We can see that along these two lines, γ is indeed quantized to $1/2$ and 0 respectively, as expected. The topological result of Fuchs *et al.*²⁹ can be seen along the horizontal $\eta = 1$ line of the upper panel. Clearly in the more general case, the same topological arguments made in that case, relating γ to a winding number, no longer apply, as γ is no longer quantized. Moving away from the horizontal line at $\eta = 1$ corresponds to the breaking of particle-hole symmetry. Moving away from the line $\Delta = 0$ can correspond to breaking inversion or time reversal symmetry, depending on the basis, if the low energy theory Eq. (16) is applicable at a high symmetry point in the Brillouin zone. In this particular regime, and considering just a single band, we recover the result of Mikitik and Sharlai,⁴⁶ that $\gamma = 0$ irrespective of the extent of particle-hole asymmetry. However, in more general systems, this does not correspond necessarily to the breaking of any particular symmetry. A prominent example is graphene with a staggered sub lattice potential, where the symmetry being broken is a sublattice one⁴⁰.

So we see that in the general case, if either of the two symmetries are retained, such that $\Delta = 0$ or $\eta = 0$ or 1 , γ is a constant, and independent of energy. If both are simultaneously broken, then the phase offset is a function of the gap (external field), the chemical potential, and the normal-fermion–Dirac fermion energy scale mv_F^2 .

B. Cyclotron effective mass

Using the temperature dependence of the magnitude of the magnetisation at fixed field, one can fit the prefactor in Eq. (14) that is $\lambda/\sinh(\lambda l)$, where λ is given by Eq. (15). Usually, one can then determine the quantities m (normal fermions) or v_F (Dirac fermions). However, in our mixed system, the cyclotron effective mass is more complicated, being given by Eq. (13), where, reintroducing the inner-outer orbit index,

$$S_{\alpha,\beta}(\epsilon) = \frac{2\pi m}{\hbar^2} \left[\epsilon_\alpha + mv_F^2 \left(1 + \beta \sqrt{\frac{\Delta^2}{(mv_F^2)^2} + \frac{2\epsilon_\alpha}{mv_F^2} + 1} \right) \right], \quad (30)$$

as outlined in Fig. 2.

We can easily check that as $v_F \rightarrow 0$, we obtain the normal fermion result of $S'(\epsilon) = 2\pi m$, and by expanding to all non-zero orders as $m \rightarrow \infty$, we obtain the usual Dirac fermion result of $S'(\epsilon) = \pi\epsilon/v_F^2$.

However, we note that in the mixed case, experimentally determining Eq. (30) does not directly give m or v_F , but contains an expression with a pair of energy scales mv_F^2 , and Δ . In fact, for a mixed system such as this, we obtain from Eq. (14), $\lambda \propto \frac{dS}{d\epsilon} = 2\pi m^*$, and so we have

$$\frac{m^*}{m} = 1 - \frac{mv_F^2}{\sqrt{\Delta^2 + 2\epsilon mv_F^2 + (mv_F^2)^2}}. \quad (31)$$

In Fig. 4 we have shown the ratio of the cyclotron mass to the normal fermion mass, the relative cyclotron mass, given by

$$\frac{m^*}{m} = 1 - \frac{\eta}{\sqrt{\frac{\Delta^2}{\mu^2}(1-\eta)^2 + \eta(2-\eta)}}. \quad (32)$$

This figure shows the gap and chemical potential dependence of the cyclotron mass, highlighting that decreasing the gap or increasing the chemical potential tunes the cyclotron orbit to a more Dirac-like part of the spectrum. It also demonstrates that the interpolation between normal and Dirac fermions smoothly interpolates the relative cyclotron mass between 1 and 0. Note that the vanishing of the relative cyclotron mass at $\eta = 1$ is due to $m \rightarrow \infty$. In the Dirac limit, the cyclotron mass is $m^* = \epsilon/v_F^2$. Nevertheless, at either $\eta = 0$ or $\eta = 1$, the effective mass m^* is gap and chemical potential independent. In between however, this is not the case, and the effective mass is a function of the gap and the chemical potential.

C. Quantum oscillations and Landau level index plots

The oscillations observed in resistivity (Eq. (1)) and magnetisation (Eq. (14)) experiments have extrema at completely filled or empty Landau levels, to which we can assign integers and half integers n ($n + 1/2$). Therefore a plot of the location of the minima/maxima as a function of magnetic field can be used to identify the magnetic field values at which one has a filled/half-filled Landau level. From Eq. (1) and Eq. (14), it is clear a sensible ordinate for a plot of minima/maxima is the inverse field strength, $1/B$. To a good approximation then, (*i.e.* only taking the first term in the series in Eq. (14)), the condition for integer filled Landau levels is

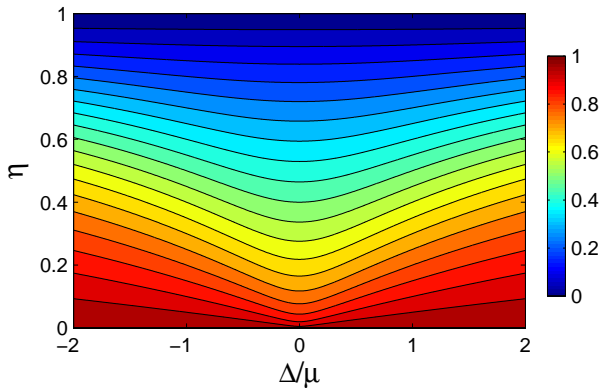


FIG. 4: (Color online) The relative cyclotron mass m^*/m as a function of Δ/μ and band bending. At $\eta = 0$, $m^* = m$. At $\eta = 1$, $m \rightarrow \infty$, so $m^*/m \rightarrow 0$. As the gap is decreased, or the chemical potential increased, the system becomes more Dirac-like. At $\eta = 0$ or $\eta = 1$, the cyclotron mass is independent of the gap/chemical potential, however in between the two this is not the case.

$$\frac{S_\alpha(\epsilon)}{2\pi\hbar eB} - \gamma_\alpha(\epsilon) = n - \Lambda, \quad (33)$$

where $\Lambda = 1/2(0)$ for the minima (maxima) of the longitudinal resistivity, and $\Lambda = 3/4(1/4)$ for the minima (maxima) of the magnetization. Further, we note that as $1/B \rightarrow 0$, the intercept of the index plot with the n -axis (offset by Λ) gives $\gamma(\epsilon)$.

In order to determine the index plot, a knowledge of both the area of the orbit, $S(\epsilon)$, and the phase offset $\gamma(\epsilon)$ is required. We have already given $\gamma(\epsilon)$ in Eq. (26), and plotted γ for all η and a range of gap parameters in Fig. 3. $S(\epsilon)$ is given in Eq. (30), however it is interesting to note the limiting cases:

$$S_\alpha(\epsilon) = \begin{cases} 2\pi m\epsilon/\hbar^2, & v_F \rightarrow 0 \text{ (Normal fermions)} \\ \pi(\epsilon^2 - \Delta^2)/\hbar^2 v_F^2, & m \rightarrow \infty \text{ (Dirac fermions)} \end{cases} \quad (34)$$

Firstly, we note that γ , Eq. (26), only varies as a function of the gap parameter in mixed normal-Dirac systems, being constant with respect to the gap in purely normal or purely Dirac systems. Therefore, for purely normal or purely Dirac systems, one expects the extrapolation of an index plot as $1/B \rightarrow 0$ to give $\gamma(\epsilon) = 0$ or $1/2$. Second, we notice that for gapless Dirac fermion and all normal fermion systems, $S(\epsilon)$ does not vary with the external field, and so the index plot is strictly linear. For a Zeeman gapped massive Dirac fermion system however, there is a nonlinearity in the index plot due to the Zeeman term $\Delta = g_s\mu_B B$. Fortunately for a material such as graphene, there is no Zeeman gap, and so the index plot reliably gives the expected intercept for relativistic fermions.¹¹ In all these cases then, correctly extrapolat-

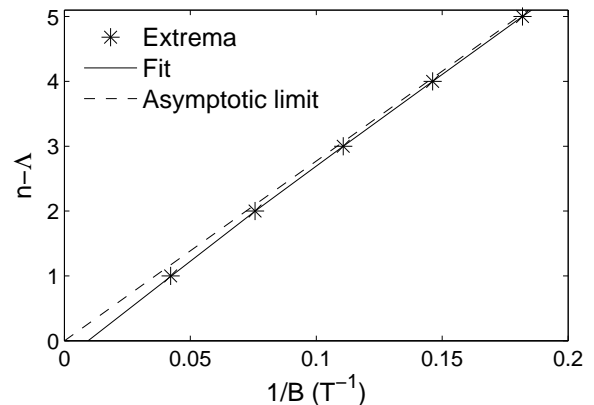


FIG. 5: (Color online) Robust determination of $\gamma_{B \rightarrow 0}$ from an index plot. The crosses represent the extremum of the resistivity or magnetisation from Eq. (1) or Eq. (14) corresponding to filled Landau levels. The solid line is the small field fit, Eq. (36). It is clear that even for a system with pronounced Zeeman splitting (here $g_s = 50$), the fit is reliable at all filling factors. The dashed line is the linearized, asymptotic fit ($d\gamma/dB = 0$ in Eq. (36)), which is asymptotically exact as $n \rightarrow \infty$. Extrapolating this line back to $1/B \rightarrow 0$ gives the topologically relevant phase offset, $\gamma_{B \rightarrow 0}$, which shows the Dirac nature of the surface states. System parameters are relevant to $\text{Bi}_2\text{Te}_2\text{Se}^{15}$: $v_F = 3.4 \times 10^5 \text{ m s}^{-1}$, $m = 0.13m_e$, $g_s = 50$.

ing the intercept at $1/B \rightarrow 0$ yields a constant field and energy independent value of γ .

In a system with non-zero Zeeman splitting, and both normal fermion and Dirac fermion terms however, $\gamma(\epsilon)$ becomes field and energy dependent, as does $S(\epsilon)$. When calculating a Landau level index plot from the maxima/minima of the oscillations (Eq. (14)) in mixed systems such as topological insulator surface states then, the index plot as a function of $|B|$ becomes uniquely nonlinear according to the energy scales of the Zeeman splitting and, as is clear from Eq. (30) and Eq. (26), mv_F^2 . In Fig. 5 this nonlinearity with increasing field can be clearly observed, and has been pointed out elsewhere^{25,26}.

It is clear from the above discussion that extrapolating an index plot to $1/B \rightarrow 0$ yields an estimate of $\gamma(\epsilon)$. However, from Eq. (26), we see that $\gamma(\epsilon)$ in the case of mixed normal fermion-Dirac fermion systems depends on the energy scales Δ and mv_F^2 . For this reason, the index plot cannot possibly discriminate between m and v_F . The cyclotron effective mass (Eq. (13)), on the other hand, intrinsically bears such a distinction. Through a combined approach of measuring the temperature dependence of the oscillation amplitudes, and thus obtaining m^* (Eq. (13)), together with index plot measurements to determine the energy scales mv_F^2 and Δ , one can determine both the normal fermion mass m , and the Dirac fermion velocity v_F .

V. USING LANDAU LEVEL INDEX PLOTS TO EXTRACT THE PHASE OFFSET

A. Taking into account the effect of a bulk Fermi surface

The quantum oscillation experiments performed thus far^{10,13–23}, tend to report a substantial bulk contribution to the measured resistivity. Although there is a bandgap at the Γ point of the surface Brillouin zone, as clearly observed with ARPES^{6,8,42}, the bulk 3D Brillouin zone is not usually gapped throughout, but has a Fermi surface.

As our Hamiltonian, Eq. (16), is merely the effective surface theory of a bulk system, we must take into account the effects of the bulk on quantum oscillation experiments. In particular, we must consider the following expression:

$$N_e = \int_{-\infty}^{\mu} \rho_b(\epsilon) d\epsilon + \int_{-\infty}^{\mu} \rho_s(\epsilon) d\epsilon \quad (35)$$

where N_e is the number of electrons, which is a constant, ρ_b is the density of states of the bulk bands, and ρ_s is the density of states of the surface bands. As we switch on a magnetic field, N_e remains constant, $\rho_s(\epsilon)$ thus changes due to the opening of a Dirac gap, and thus μ varies. Since the surface band is a two-dimensional band, of which there is only one, whereas the bulk bands are three-dimensional and there are many, the number of bulk carriers is much greater than the number of surface carriers.

Therefore, there are two distinct regimes.

1. *If there is a bulk Fermi surface*, the contribution to N_e will come almost entirely from the first term in Eq. (35), and so the chemical potential of the surface band will be dictated by the change in chemical potential of the bulk band. In the limit where the bulk Fermi surface shifts by a negligible amount, this is equivalent to taking the surface theory, Eq. (16), in the grand canonical ensemble, where μ remains constant, and the Fermi wavevector k_F , and therefore $S(\mu)$ varies.
2. *If the bulk is completely gapped*, the first, bulk, contribution to Eq. (35) remains constant, and the change in μ is dictated entirely by the surface theory. This corresponds to the case most frequently considered, where it can be shown that the Fermi wavevector remains constant (Luttinger's theorem⁵³), and thus $S(\mu)$ remains constant as μ varies.

Xiong *et. al.*²⁰ have pointed out a second subtlety in the presence of a bulk Fermi surface. They argue that when measuring the longitudinal resistivity, the contribution of the bulk resistivity demands that filled Landau levels be associated with resistivity maxima, rather than resistivity minima.

B. Extracting the phase offset at small fields

Experimental determination of the index plot in this case of mixed Dirac and normal fermions is, as we have discussed, fraught. In the presence of an unknown gap, an intercept with n yields a non-quantized value of γ which can sit anywhere on an equal- γ contour in Fig. 3. Furthermore, if the gap is from Zeeman splitting, it is linearly dependent upon B , and so, as pointed out by Taskin and Ando²⁶ as well as Seradjeh, Wu and Phillips²⁵, and shown in Fig. 5, will not produce a straight line in the index plot as a function of inverse field strength.

As the phase offset $\gamma(\epsilon)$ is only non-constant when the system is both gapped *and* the electrons are mixed normal and Dirac fermions, we can use this fact to determine whether the system has a gap at zero field. It is interesting to note that due to both of these stipulations being simultaneously required, this ability of quantum oscillations to extract an intrinsic gap is only possible in the unique mixed normal-Dirac systems we are considering here.

In the case of a system with no intrinsic band-gap, we would like to measure $\gamma_{B \rightarrow 0} = 0$, the ‘topological’ result for Dirac fermions. If the system has a tunnel-split gap, or some other more exotic gap, then $\gamma_{B=0} \neq 0$.

In order to circumvent the difficulties outlined above, and in order to systematically obtain a reliable value for the topological phase offset, or a measure of the intrinsic band-gap, we propose the following procedure. Starting with Eq. (33), we make a small field expansion and rearrange to obtain

$$n - \Lambda \approx \frac{B_0}{B} - \gamma_{B \rightarrow 0} - C \frac{d\gamma}{dB} \Big|_{B \rightarrow 0} B, \quad (36)$$

where

$$B_0 = \frac{S(\epsilon)|_{B \rightarrow 0}}{2\pi\hbar e} \quad (37)$$

is the area enclosed by the cyclotron orbit with no Zeeman correction, and

$$\frac{d\gamma_\alpha(\epsilon)}{dB} \Big|_{B \rightarrow 0} = \frac{\alpha g_s \mu B}{2mv_F^2 \sqrt{\frac{2\epsilon}{mv_F^2} + 1}}. \quad (38)$$

The constant C is, in general, unknown. In case 1 outlined in the previous subsection, where there is a bulk Fermi surface *and* the change in μ with increasing magnetic field is negligibly small, $S(\epsilon)$ varies as a function of magnetic field. The variation of $S(\epsilon)$ with magnetic field can be approximated by expanding Eq. (30) with respect to the field. The second term in such an expansion, which goes as B^2 , is $\propto d\gamma/dB|_{B \rightarrow 0}$. In this case then, C has a contribution from the gradient of γ , as well as a contribution from the change in the area of the Fermi surface at μ , which is proportional to the gradient of γ

and the ratio of the Zeeman energy ($\Delta_Z = g_s \mu_B B$) to the cyclotron energy of the normal fermion ($\hbar\omega_0 = \hbar eB/m$). In case 2, $S(\epsilon)$ is a constant, and so $C = 1$. Therefore

$$C = \begin{cases} 1 + \frac{\Delta_Z}{\hbar\omega_0}, & \mu \text{ constant (bulk Fermi surface),} \\ 1, & S(\epsilon) \text{ constant (bulk gap).} \end{cases} \quad (39)$$

The topologically relevant quantity is $\gamma_{B \rightarrow 0}$, which is the intercept of Eq. (36) with the $n - \Lambda$ axis in the limit $d\gamma/dB \rightarrow 0$.

Our proposal is thus as follows:

1. Plot the experimentally obtained extrema in the resistivity or the magnetisation as a function of $1/B$.
2. Fit the data to the fitting function

$$n - \Lambda = \frac{B_0}{B} + A_1 + A_2 B, \quad (40)$$

where B_0 , A_1 , and A_2 are constants.

3. The asymptotic low field limit ($B \rightarrow 0$) is equivalent to $A_2 \rightarrow 0$ and yields a straight line, whose intercept with the n axis is $\gamma_{B \rightarrow 0}$. Therefore, the topologically relevant phase offset is A_1 . If $A_1 = 0$, the surface states are gapless, and contain a Dirac component with a Berry phase of π . If $A_1 \neq 0$, then the system may have an intrinsic band-gap.

Eq. (36), together with theoretically obtained minima of Eq. (1) or Eq. (14), is plotted in Fig. 5 for typical parameter values. The fitting function is seen to be a good fit for all n . The topologically relevant asymptotic form of Eq. (36) has also been plotted in Fig. 5, where $\gamma_{B \rightarrow 0} = 0$, as expected for topological insulator surface states with no intrinsic band-gap.

We emphasise that producing a straight line fit to the experimental points, rather than following the procedure outlined above, will only yield a reasonable estimate of $\gamma_{B \rightarrow 0}$ for very large n . As can be seen from Fig. 5, the asymptotic approach of the data to the straight line fit is slow (approaching as $1/B^{-1}$). A more reliable method is to fit Eq. (40) to the data, and in this way extract the topologically relevant zero field phase offset.

VI. COMPARISON WITH EXISTING EXPERIMENTS

As has been pointed out by Taskin and Ando²⁶, the nonlinearity of the index plots for large B is evident in many existing studies, and the extrapolation to $1/B \rightarrow 0$ by fitting a straight line through the data points consistently yields $\gamma \neq 0, 1/2$ (see Table I). It is also possible that for certain values of g_s , or external fields, the index plot will curve so much that the extrapolation spuriously yields $\gamma = 1/2$ for a topological insulator surface state.

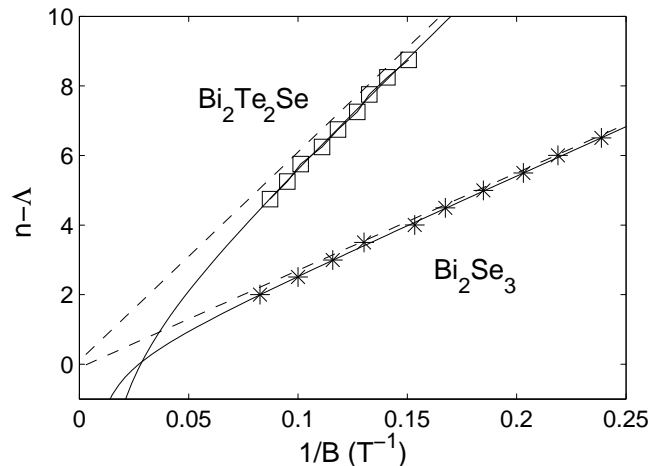


FIG. 6: Determination of the zero field phase offset $\gamma_{B \rightarrow 0}$ using the fitting function Eq. (40) (solid lines) on experimental data for $\text{Bi}_2\text{Te}_2\text{Se}$ ¹⁵, and Bi_2Se_3 ¹⁰. For $\text{Bi}_2\text{Te}_2\text{Se}$, we have shifted n index by $1/2$, following Xiong *et al.*²⁰, and obtain $\gamma_{B \rightarrow 0} = -0.1$, whereas a linear fit to the data yields $\gamma_{B \rightarrow 0} = -0.78$. For Bi_2Se_3 , we obtain $\gamma_{B \rightarrow 0} = 0.1$, whereas a linear fit yields $\gamma_{B \rightarrow 0} = -0.36$. The dashed lines are the asymptotic plots of Eq. (36), with $A_2 = 0$, whose $n - \Lambda$ intercept gives the topologically important zero field phase offset.

In fact Analytis *et al.*¹⁴ obtained such a result with their sample 2 (see Table I). It is clear from our results that these findings are to be expected, and the problem may be systematically circumvented by fitting Eq. (40) to the low field data and thus obtaining a reliable estimate of $\gamma_{B \rightarrow 0}$, as outlined above.

In Fig. 6 we have performed just such an analysis for two existing experimental studies on $\text{Bi}_2\text{Te}_2\text{Se}$ ¹⁵, and Bi_2Se_3 ¹⁰. Following the discussion of Xiong *et al.*²⁰, we have shifted the index identification n in the former by $1/2$. The reason for this being that the bulk contribution to the longitudinal resistivity causes the maxima, rather than the minima, to be associated with a completely filled Landau level. If this is the case, then a linear extrapolation of the data yields an intercept of $\gamma_{B \rightarrow 0} = -0.78$. On the other hand, using Eq. (40), our fit becomes

$$n - \frac{1}{2} \approx \frac{60}{B} + 0.1 - 0.05B \quad (41)$$

Comparing with Eq. (36) then, we find $B_0 = 60$ T, in agreement with the value obtained in the original paper¹⁵, and $\gamma_{B \rightarrow 0} = 0.1$, which is close to the expected value of 0. From Eq. (38), and the expression for C at fixed μ , Eq. (39), we see that if we use known values of m and v_F , we can estimate the g-factor from the third term in the above result. Using this value we obtain $g_s \approx 60$ for $\eta = 0.39$, which is in broad agreement with similar estimates given elsewhere^{14,26}.

Turning to the case of Bi_2Se_3 ¹⁰, we obtain

$$n - \frac{1}{2} \approx \frac{28}{B} - 0.1 - 0.018B \quad (42)$$

Again, we obtain a good agreement with $B_0 = 28$ T, and a zero phase offset of $\gamma_{B \rightarrow 0} = 0.1$, whereas a linear fit yields $\gamma_{B \rightarrow 0} = -0.36$. Using the material parameters of Bi_2Se_3 from Table II, we obtain broad agreement with estimates given elsewhere, namely $g_s \approx 50$ for $\eta = 0.54$.

This brief comparison with experiment highlights the need for further experiments on higher purity samples with smaller Dingle temperatures. This will enable extending the index plots to lower fields.

VII. APPLICATION TO SPINTRONICS

For η small, the Hamiltonian Eq. (16) corresponds to a typical spintronics system: a two dimensional electron gas, such as GaAs and InAs quantum wells with Rashba spin-orbit interaction.³⁷ For v_F small, the two bands become nearly degenerate, and both contribute to quantum oscillations, *i.e.* the sum over α must be completed in Eq. (14).

A robust treatment of these systems is not within the scope of the current work, as inter-band effects contribute a significant third portion to the oscillations^{54,55}, on top of the oscillations of the two intra-bands, and so a third term is required in Eq. (14), as inter-band tunnelling becomes possible.

However, the results of the present work do allow one particularly striking prediction for spintronic systems. According to Eq. (26), and Fig. 3, for *any* finite Dirac velocity, or in this particular case, Rashba spin-orbit interaction, as $\Delta \rightarrow 0$, $\gamma \rightarrow 0$. For very small Rashba terms though, this transition from $\gamma \approx \pm 1/2$ to $\gamma = 0$ becomes almost step-like. Therefore, for all but the tiniest of Zeeman fields, one might expect to measure $\gamma = 1/2$, even though the $B \rightarrow 0$ limit indeed gives $\gamma = 0$. For low fields, the intra-band components dominate⁵⁶, and so it is expected that in the limit $B \rightarrow 0$, the model outlined here without inter-band scattering will become relevant.

Experimental observation of an index plot with intercept consistent with $\gamma = 0$ in a 2DEG with small Rashba splitting would be a powerful confirmation of the current work.

VIII. CONCLUSIONS

We have developed a semi-classical theory of quantum oscillations in general particle-hole symmetry broken sys-

tems. In particular, we have applied the formalism to mixed normal fermion – Dirac fermion systems, which is particularly relevant to topological insulator surface states.

By properly treating the pseudo-spin magnetic moment, we have shown that the phase offset observed in quantum oscillation experiments is, in general, not quantized. We found that the quantized result can be expected in gapless systems, or in particle-hole symmetric systems, in agreement with previous studies. However, we have shown that if particle-hole symmetry is broken, and there is a gap, then the phase offset is not quantized.

We have developed a protocol which allows one to determine the material properties of topological insulator surface states, in particular the normal fermion mass, the Dirac fermi velocity, the g-factor, and the intrinsic gap, by using quantum oscillation experiments. In particular, the effective mass cannot be naively applied to give the Fermi velocity, but is corrected due to Zeeman splitting and the energy scale mv_F^2 . Furthermore, the observed nonlinear index plots can be fit to a simple function at small fields. From this, one can read off the phase offset at zero field, and directly determine the intrinsic gap, or else regain the ‘topological’ result of zero phase offset, as expected where there is no mixing of normal and Dirac fermions.

The unique interplay of the normal fermion mass and the Dirac Fermi velocity to create an energy scale mv_F^2 , together with the Zeeman or intrinsic gap, add rich subtleties to quantum oscillation experiments that allow this already powerful tool to probe material properties in new ways.

In future studies we will focus on topologically significant gap phenomena, such as the topological exciton condensate,²⁸ and how quantum oscillation experiments can be used to identify and probe these topologically non-trivial regimes.

Acknowledgments

We thank J. Kokalj for critical readings of the manuscript and helpful discussions. We also thank O. Sushkov, A. Hamilton, and T. Li for constructive feedback on the results, and especially J.N. Fuchs for providing critical feedback of the preprint. Financial support was received from a UQ Postdoctoral Fellowship (ARW) and an Australian Research Council Discovery Project (RHM).

* Electronic address: a.wright7@uq.edu.au

¹ C.L. Kane and E.J. Mele, *Phys. Rev. Lett.* **95**, 226801

(2005).

² M. Z. Hasan and C. L. Kane, *Rev. Mod. Phys.* **82**, 3045

- (2010).
- ³ X.-L. Qi and S.-C. Zhang, *Rev. Mod. Phys.* **83**, 1057 (2011).
 - ⁴ M. König, S. Wiedmann, C. Brüne, A. Roth, H. Buhmann, L.W. Molenkamp, X.-L. Qi, and S.-C. Zhang, *Science* **318**, 766 (2007).
 - ⁵ A. Roth, C. Brüne, H. Buhmann, L.W. Molenkamp, J. Maciejko, X.-L. Qi, and S.-C. Zhang, *Science* **325**, 294 (2009).
 - ⁶ Y. L. Chen, J. G. Analytis, J.-H. Chu, Z. K. Liu, S.-K. Mo, X. L. Qi, H. J. Zhang, D. H. Lu, X. Dai, Z. Fang, S. C. Zhang, I. R. Fisher, Z. Hussain and Z.-X. Shen, *Science* **325**, 178 (2009).
 - ⁷ D. Hsieh, Y. Xia, D. Qian, L. Wray, J. H. Dil, F. Meier, J. Osterwalder, L. Patthey, J. G. Checkelsky, N. P. Ong, A. V. Fedorov, H. Lin, A. Bansil, D. Grauer, Y. S. Hor, R. J. Cava and M. Z. Hasan, *Nature* **460**, 1101 (2009).
 - ⁸ D. Hsieh, Y. Xia, L. Wray, D. Qian, A. Pal, J. H. Dil, J. Osterwalder, F. Meier, G. Bihlmayer, C. L. Kane, Y. S. Hor, R. J. Cava and M. Z. Hasan, *Science* **323**, 5916 (2009).
 - ⁹ T. Champel and V. P. Mineev, *Philos. Mag. B* **81**, 55 (2001).
 - ¹⁰ D.-X. Qu, Y. S. Hor, J. Xiong, R. J. Cava, and N. P. Ong, *Science* **329**, 821 (2010).
 - ¹¹ K. S. Novoselov, A. K. Geim, S. V. Morozov, D. Jiang, M. I. Katsnelson, I. V. Grigorieva, S. V. Dubonos and A.A. Firsov, *Nature* **438**, 197 (2005).
 - ¹² Y. Zhang, Y.-W. Tan, H. L. Stormer, and P. Kim, *Nature* **438**, 201 (2005).
 - ¹³ A.A. Taskin, K. Segawa, and Y. Ando, *Phys. Rev. B* **82**, 121302(R) (2010).
 - ¹⁴ J.G. Analytis, R.D. McDonald, S.C. Riggs, J.-H. Chu, G.S. Boebinger, and I.R. Fisher, *Nat. Phys.* **6**, 960 (2010).
 - ¹⁵ Z. Ren, A.A. Taskin, S. Sasaki, K. Segawa and Y. Ando, *Phys. Rev. B* **82**, 241306(R) (2010).
 - ¹⁶ A.A. Taskin, Z. Ren, S. Sasaki, K. Segawa, and Y. Ando, *Phys. Rev. Lett.* **107**, 016801 (2011).
 - ¹⁷ C. Brüne, C. X. Liu, E. G. Novik, E. M. Hankiewicz, H. Buhmann, Y. L. Chen, X. L. Qi, Z. X. Shen, S. C. Zhang, and L. W. Molenkamp, *Phys. Rev. Lett.* **106**, 126803 (2011).
 - ¹⁸ M. Veldhorst, M. Snelder, M. Hoek, T. Gang, V. K. Guduru, X. L. Wang, U. Zeitler, W. G. van der Wiel, A. A. Golubov, H. Hilgenkamp, and A. Brinkman, *Nat. Mat.* **11**, 417 (2012).
 - ¹⁹ L. He, F. Xiu, M. Teague, W. Jiang, Y. Fan, X. Kou, M. Lang, Y. Wang, G. Huang, N.-C. Yeh, and K.L. Wang, *Nano Lett.* **12**, 1486 (2012).
 - ²⁰ J. Xiong, Y. Luo, Y.H. Khoo, S. Jia, R. J. Cava, and N. P. Ong, *Phys. Rev. B* **86**, 045314 (2012).
 - ²¹ J. Xiong, A.C. Petersen, D. Qu, Y.S. Hor, R.J. Cava, N.P. Ong, *Physica E* **44**, 917 (2012).
 - ²² B. Sacépe, J.B. Oostinga, J. Li, A. Ubaldini, N.J.G. Couto, E. Giannini, and A.F. Morpugo, *Nat. Comm.* **2**, 575 (2011).
 - ²³ A. A. Taskin, S. Sasaki, K. Segawa, and Y. Ando, *Phys. Rev. Lett* **109**, 066803 (2012).
 - ²⁴ Z. Ren, A. A. Taskin, S. Sasaki, K. Segawa, and Y. Ando, *Phys. Rev. B* **85**, 155301 (2012).
 - ²⁵ B. Seradjeh, J. Wu, and P. Phillips, *Phys. Rev. Lett.* **103**, 136803 (2009).
 - ²⁶ A.A. Taskin and Y. Ando, *Phys. Rev. B* **84**, 035301 (2011).
 - ²⁷ B. Seradjeh, J. E. Moore, and M. Franz, *Phys. Rev. Lett.* **103**, 066402 (2009).
 - ²⁸ G.Y. Cho and J.E. Moore, *Phys. Rev. B* **84**, 165101 (2011).
 - ²⁹ J.N. Fuchs, F. Piéchon, M.O. Goerbig, and G. Montambaux, *Eur. Phys. J. B* **77**, 351 (2010).
 - ³⁰ L.M. Roth, *Phys. Rev.* **145**, 434 (1966).
 - ³¹ M.V. Berry, *Proc. R. Soc. Lond. A* **392**, 45 (1984).
 - ³² D. Xiao, M.-C. Chang, and Q. Niu, *Rev. Mod. Phys.* **82**, 1959 (2010).
 - ³³ G.P. Mikitik and Y.V.Sharlai, *Phys. Rev. Lett.* **82**, 2147 (1999).
 - ³⁴ L. Fu, *Phys. Rev. Lett.* **103**, 266801 (2009).
 - ³⁵ C.-X. Liu, X.-L. Qi, H. J. Zhang, X. Dai, Z. Fang, and S.-C. Zhang, *Phys. Rev. B* **82**, 045122 (2010).
 - ³⁶ I.A. Luk'yanchuk and Y. Kopelevich, *Phys. Rev. Lett.* **93**, 166402 (2004).
 - ³⁷ I. Žutić, H. Fabian, and S. Das Sarma, *Rev. Mod. Phys.* **76**, 323 (2004).
 - ³⁸ A.P. Schnyder, S. Ryu, A. Furusaki, and A.W.W. Ludwig, *Phys. Rev. B* **78**, 195125 (2008).
 - ³⁹ Z. Wang, Z.-G. Fu, S.-X. Wang, and P. Zhang, *Phys. Rev. B* **82**, 085429 (2010).
 - ⁴⁰ G.W. Semenoff, V. Semenoff, and F. Zhou, *Phys. Rev. Lett.* **101**, 087204 (2008).
 - ⁴¹ J. Linder, T. Yokoyama, and A. Sudbø, *Phys. Rev. B* **80**, 205401 (2009).
 - ⁴² Y. Xia, D. Qian, D. Hsieh, L. Wray, A. Pal, H. Lin, A. Bansil, D. Grauer, Y. S. Hor, R. J. Cava and M. Z. Hasan, *Nat. Phys.* **5**, 398 (2009).
 - ⁴³ Y. L. Chen, J. G. Analytis, J.-H. Chu, Z. K. Liu, S.-K. Mo, X. L. Qi, H. J. Zhang, D. H. Lu, X. Dai, Z. Fang, S. C. Zhang, I. R. Fisher, Z. Hussain, and Z.-X. Shen, *Science* **325**, 178 (2009).
 - ⁴⁴ S. Adam, E.H. Hwang, and S. Das Sarma, *Phys. Rev. B* **85**, 235413 (2012).
 - ⁴⁵ D. Kim, S. Cho, N.P. Butch, P. Syers, K. Kirshenbaum, S. Adam, J. Paglione, M.S. Fuhrer, *Nat. Phys.* **8**, 460 (2012).
 - ⁴⁶ G.P. Mikitik and Y.V.Sharlai, *Phys. Rev. B* **85**, 033301 (2012).
 - ⁴⁷ C.-X. Liu, H.J. Zhang, B. Yan, X.-L. Qi, T. Frauenheim, X. Dai, Z. Fang, and S.-C. Zhang, *Phys. Rev. B* **81**, 041307(R) (2010).
 - ⁴⁸ Y. Zhang, K. He, C.-Z. Chang, C.-L. Song, L.-L. Wang, X. Chen, J.-F. Jia, Z. Fang, X. Dai, W.-Y. Shan, S.-Q. Shen, Q. Niu, X.-L. Qi, S.-C. Zhang, X.-C. Ma and Q.-K. Xue, *Nat. Phys.* **6**, 584 (2010).
 - ⁴⁹ H.-Z. Lu, W.-Y. Shan, W. Yao, Q. Niu, and S.-Q. Shen, *Phys. Rev. B* **81**, 115407 (2010).
 - ⁵⁰ T. Sato, K. Segawa, K. Kosaka, S. Souma, K. Nakayama, K. Eto, T. Minami, Y. Ando and T. Takahashi, *Nat. Phys.* **7**, 840 (2011).
 - ⁵¹ X.-L. Qi, T.L. Hughes and S.-C. Zhang, *Phys. Rev. B* **78**, 195424 (2008).
 - ⁵² D. Schoenberg, *Magnetic Oscillations in Metals*, Cambridge University Press, Cambridge, 1984.
 - ⁵³ J.M. Luttinger, *Phys. Rev.* **119**, 1153 (1960).
 - ⁵⁴ P.T. Coleridge, *Semicond. Sci. Technol.* **5**, 961 (1990).
 - ⁵⁵ M. E. Raikh and T. V. Shahbazyan, *Phys. Rev. B* **49**, 5531 (1994).
 - ⁵⁶ T.H. Sander, S.N. Holmes, J.J. Harris, D.K. Maude, and J.C. Portal, *Phys. Rev. B* **58**, 13856 (1998).